Supplement 1 Cross-calibration of MCPC

During the 2024 field campaign, three MCPCs units were installed to sample aerosols, recognised by their serial numbers: 23, 31, and 134. The combination of MCPC aerosol measurement can be found in Table S1. Although the residence time was tested to be the same between aerosols passing through the unheated inlet and the heated inlet with the thermodenuder, a time delay was still observed. The time delays between 2 MCPCs were corrected by aligning the time at which the aircraft sampled the vessel-generated SSA_a plume, assuming that the peak values of both non-volatile and total aerosol number concentrations occurred simultaneously. Both MCPC 23 and 134 datasets were calibrated against the MCPC 31 for consistency before the thermodenuder was turned on (Figure S1). All flights listed in Table S1 were checked within the housekeeping thresholds and data errors.

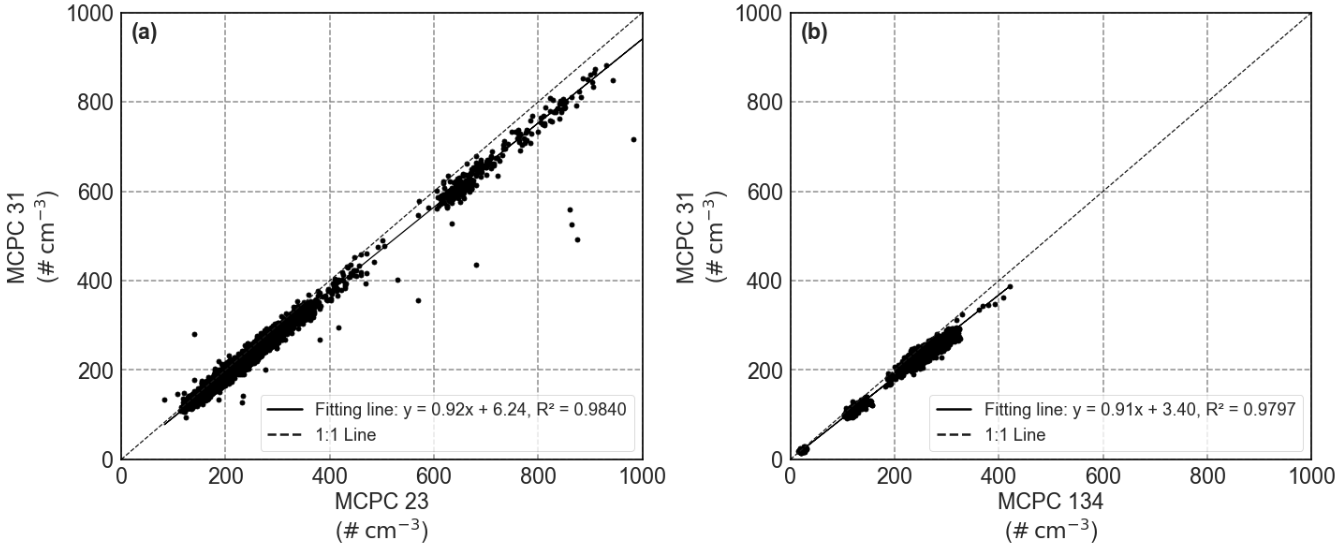

Figure S1 Cross-calibration of MCPC (a) serial no.23 and no.31, and (b) serial no.134 and no.31, using data from all flights listed in Table S1. MCPC 31 measures isokinetic total aerosols in the left and isokinetic non-volatile in the right, while (a) MCPC 23 and (b) MCPC 31 measured isokinetic non-volatile and total aerosols, respectively.

Table S1 MCPC serial number of each flight to measure non-volatile and total aerosols and the cross-calibration equation between 2 MCPCs

Flight ID	MCPC Non-Volatile/ Total Aerosol Serial No.	Cross-calibration Equation	R^2
20240206	23/31		
20240207_F1	23/31		
20240208_F1	23/31		
20240208_F2	23/31		
20240209_F1	23/31	y(31) = 0.92x + 6.24	0.9840
20240209_F2	23/31		
20240210	23/31		
20240212_F1	23/31		
20240213_F1	23/31		
20240215_F1	23/31		
20240221_F1	31/134		
20240223_F1	31/134		
20240223_F2	31/134	y(31) = 0.91x + 3.4	0.9797
20240225	31/134		
20240226_F2	31/134		

Supplement 2 Sensitivity test of SD Method

Different sets of ∂ and σ were applied to evaluate the performance of the SD method (see Table S2). We selected three ranges of datasets to calculate σ, specifically the data for each flight between the 10th and 90th percentiles, 25th and 75th percentiles, and 30th and 70th percentiles. The value of σ calculated between the 10th and 90th percentiles was generally higher than that calculated between the other two percentile ranges. For most flights, the σ value of the 10th and 90th percentiles were even more than twice as high as the value between the 25th and 75th percentiles. For the threshold parameter ∂, we selected values of 1 and 2. A lower value ∂ resulted in more flagged spikes, while choosing the value of 2 significantly reduced the number. The most significant reduction tended to occur in the 10th ~ 90th percentile range, with some exceptions that fell into the other two percentile ranges. This shows that spike detection is more sensitive to the value of σ than the threshold parameter ∂. In other words, if the dataset used to calculate σ did not accurately reflect the data distribution, then adjusting ∂ would have a limited effect on the outcome of spike detection.

The number concentrations of non-volatile and total aerosols responded differently to the SD method. Generally, the non-volatile aerosol number concentration was flagged with fewer spikes compared to the total aerosol number concentration across all flights. For more than half of the flights, total aerosol number concentration exhibited higher values of σ than non-volatile aerosols, particularly when σ was calculated using the dataset between the 10th and 90th percentiles. Aerosol spikes, if primarily driven by non-volatile sources, would result in more abrupt changes in non-volatile aerosol number concentration than in total aerosol number concentration. Including these abrupt changes to calculate σ would lead to higher values of σ and, consequently, fewer spikes. These results suggest that the dataset percentile range used for σ calculation should be adjusted differently for total and non-volatile aerosols to identify spikes effectively. Additionally, variations in background aerosol number concentration influenced how the time-series data of aerosol number concentrations would respond to the SD method. Background aerosols varied between flights and changed with sampling altitude within each flight. As a result, this variation could limit the portion of smoothly varying background data available for calculating σ, yielding fewer spikes being flagged. Overall, the SD method was effective in flagging spikes in aerosol number concentration, as shown in Figure S2. The SD method successfully flagged most spikes caused by sprayed SSA_a for both total and non-volatile aerosol number concentration. However, the SD method did not flag those spikes as the aircraft flew out of the SSA_a plume and before the number concentration dropped to the background aerosol level. Therefore, evaluating the SD method is critically important when a known source exists. Accordingly, a "spike" was identified for each flight whenever the non-volatile or total aerosol number concentration was flagged by the SD method. The non-volatile aerosol ratio of these flagged "spikes" will be checked using the mixing ratio model, also referred to as the "tracer" method.

In selecting the percentile range to calculate the SD for each flight, we initially followed the approach of El Yazidi et al. (2018) using the fixed 25th ~ 75th percentile range. We initially evaluated whether this percentile range was appropriate for all flights through histogram analysis, cumulative distribution functions, plume concentration boundaries and background concentration boundaries within identified plume sampling periods, and statistical metrics (mean, SD, and coefficient of variation (CV)). However, these analyses could not consistently identify an appropriate percentile range across all flights. Therefore, a flightspecific evaluation was performed using a series of percentile ranges, including 10th ~ 90th, 20th ~ 80th, 25th ~ 75th, 30th ~ 70th, 35th ~ 65th, and 40th ~ 60th. For each range, we calculated the mean, SD, CV, and flagged spikes percentage.

A representative example is shown in Figure S2 and S3 for the first flight on February 21st, 2024. For the total aerosol number concentration, all percentile ranges produced CV values lower than 10%, whereas the percentage of SD-flagged spikes increased markedly from 5.01% for the 10th ~ 90th percentile range to 73.68% for the 40th ~ 60th percentile range, suggesting progressively stronger spike detection as the percentile range narrowed. The identified plume periods accounted for 3.41% of the flight duration. Among all percentile ranges, the 10th ~ 90th percentile range produced the most reasonable agreement with the known plume period without introducing obvious over-detection of spikes. This selection was further verified by visual inspection of the time series, where identified spikes corresponded well to the identified plume periods while the remaining aerosol number concentrations were relatively stable. Hence, the 10th ~ 90th percentile range was selected for the total aerosol number concentration of this flight.

The non-volatile aerosol number concentration was subsequently evaluated. During the flight, the variability of non-volatile aerosol number concentration was generally less than the total aerosol number concentration (Table S2). In addition, the transition periods when the thermodenuder was switched on and off introduced variability at the beginning and end of the flight. The duration of these transitions differed among all flights. Consequently, the percentile range was first determined using the total aerosol number concentration, which flagged most of plume-related spikes, and was subsequently refined for the non-volatile aerosol number concentration. For this flight, the 25th ~ 75th percentile provided a reasonable representation of the flagged spikes despite a higher CV (16.83%) and was selected for calculating the SD.

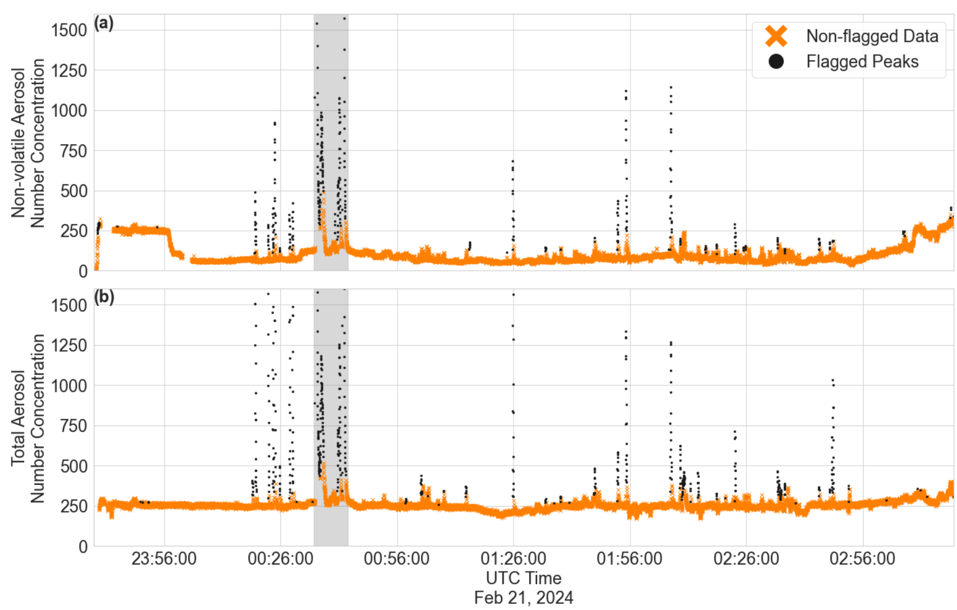

Figure S2 Time series of a) non-volatile and b) total aerosol number concentration during 2024 February 21st, where grey indicates the plume sampling period

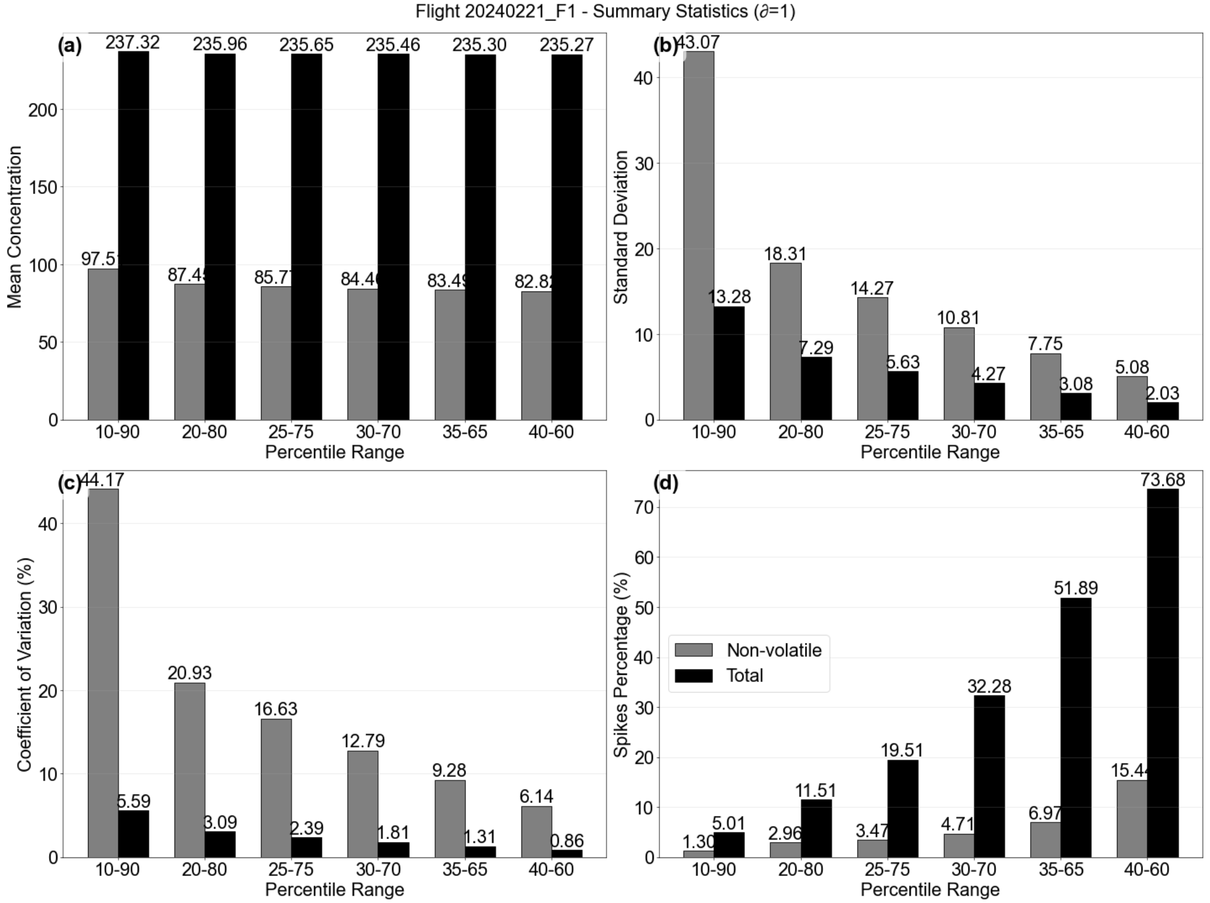

Figure S3 Statistical evaluation of percentile ranges for first flight on February 21st, 2024, (a) mean, (b) SD, (c) CV, and (d) spikes percentage for each percentile range

Table S2 Sensitivity test of the standard deviation method for each flight

Flight ID	MCPC Measurement	10% ~ 90%			25% ~ 75%			30% ~ 70%		
		σ	**∂=1**	**∂=2**	**Σ**	**∂=1**	**∂=2**	**σ**	**∂=1**	**∂=2**
20240206	Total Aerosol	141.5544	1.28	0.83	68.8957	2.02	1.7	55.9262	2.32	1.99
	Non-volatile Aerosol	129.7501	0.37	0.28	58.4957	0.59	0.5	45.4002	0.77	0.61
20240207_F1	Total Aerosol	94.5481	0.24	0.09	58.6237	0.51	0.26	47.5534	0.54	0.37
	Non-volatile Aerosol	66.6154	0.14	0.05	44.2755	0.15	0.14	36.6487	0.22	0.14
20240208_F1	Total Aerosol	24.9652	1.42	0.86	14.4633	2.83	1.82	11.568	3.99	2.46
	Non-volatile Aerosol	28.4904	0.45	0.3	17.1572	1.19	0.68	13.5588	1.82	0.99
20240208_F2	Total Aerosol	27.062	1.78	1.13	16.1214	4.24	2.27	12.7343	5.92	3.48
	Non-volatile Aerosol	24.2821	0.49	0.37	11.5802	2.22	1.11	8.2498	3.79	2.11
20240209_F1	Total Aerosol	38.8411	2.34	1.39	20.4935	4.24	2.96	16.4142	5.68	3.83
	Non-volatile Aerosol	36.8438	1.84	1.38	18.3944	4.07	2.83	14.5374	5.39	3.69
20240209_F2	Total Aerosol	45.5401	0.95	0.65	27.2738	1.91	1.24	19.7438	2.96	1.9
	Non-volatile Aerosol	57.2692	0.45	0.11	29.327	1.38	0.94	18.0765	2	1.57
20240210	Total Aerosol	30.0082	0.88	0.66	17.226	1.64	1.16	13.5435	2.42	1.51
	Non-volatile Aerosol	20.3596	0.72	0.6	10.9261	1.54	0.95	8.6057	2.89	1.18
20240212_F1	Total Aerosol	23.6508	1.81	1.32	12.3355	5.98	3.21	9.7246	8.09	5.28
	Non-volatile Aerosol	25.0983	0.72	0.59	13.2795	2.21	1	10.6571	2.77	2.08
20240213_F1	Total Aerosol	23.7862	2.08	1.09	13.7542	3.67	2.6	10.5577	5.22	3.61
	Non-volatile Aerosol	15.8692	1.14	0.63	7.8217	3.1	1.77	6.0446	4.89	2.96
20240215_F1	Total Aerosol	49.6971	2.18	1.22	33.3473	4.15	2.53	28.083	5.03	3.24
	Non-volatile Aerosol	47.4732	0.97	0.32	34.409	2.04	0.92	30.2393	2.23	1.18
20240221_F1	Total Aerosol	13.2776	5.01	4.11	5.6296	19.51	9.4	4.2719	32.28	16.12
	Non-volatile Aerosol	43.0692	1.3	0.92	14.2662	3.47	2.63	10.806	4.71	3.52
20240223_F1	Total Aerosol	30.4064	3.81	2.91	14.7885	6.13	5	10.9503	8.63	5.99
	Non-volatile Aerosol	56.1068	2.15	1.8	26.0421	3.64	2.94	17.3033	5.12	3.93
20240223_F2	Total Aerosol	13.6631	4.24	3.73	4.3086	28.08	13.12	3.2343	43.36	24.18
	Non-volatile Aerosol	58.4708	0.16	0.08	38.3655	0.5	0.16	25.495	1.33	0.65
20240225	Total Aerosol	46.0687	0.51	0.06	32.8942	0.74	0.56	28.2474	0.93	0.69
	Non-volatile Aerosol	26.4494	0.12	0	15.9835	0.89	0.24	12.1474	2.29	0.8
20240226_F2	Total Aerosol	20.3265	1.15	0.46	11.9422	2.82	1.77	9.3456	4.4	2.27
	Non-volatile Aerosol	21.0871	0.81	0.37	13.8737	1.87	0.91	11.3311	2.95	1.4

Table S3 Dataset to calculate the standard deviation, the number of ∂, CV, SD-flagged spikes percentage, and identified plume percentage for each flight

Flight ID	MCPC Non-volatile Aerosols				MCPC Total Aerosols				Plume Percentage (%)
	SD	∂	CV (%)	Spikes percentage (%)	SD	∂	CV (%)	Spikes percentage (%)	
20240206	$40^{th} \sim 60^{th}$	1	5.85	1.9	$30^{th} \sim 70^{th}$	1	9.4	2.32	2.06
20240207_F1	$40^{th} \sim 60^{th}$	1	11.53	0.87	$40^{th} \sim 60^{th}$	1	9.47	1.52	0.4
20240208_F1	$35^{th} \sim 65^{th}$	1	12.3	2.61	$25^{th} \sim 75^{th}$	1	8.1	2.84	0.2
20240208_F2	$30^{th} \sim 70^{th}$	1	12.91	3.79	$25^{th} \sim 75^{th}$	1	9.47	4.24	1.4
20240209_F1	$30^{th} \sim 70^{th}$	1	17.6	5.39	$25^{th} \sim 75^{th}$	1	10.37	4.24	1.19
20240209_F2	$35^{th} \sim 65^{th}$	1	13.9	2.97	$30^{th} \sim 70^{th}$	1	9.98	2.96	2.5
20240210	$30^{th} \sim 70^{th}$	1	8.8	2.89	$30^{th} \sim 70^{th}$	1	6.69	2.42	0.9
20240212_F1	$25^{th} \sim 75^{th}$	1	18.17	2.21	$25^{th} \sim 75^{th}$	1	7.8	5.98	1.26
20240213_F1	$25^{th} \sim 75^{th}$	1	12.53	3.1	$25^{th} \sim 75^{th}$	1	11.06	3.67	0.66
20240215_F1	$40^{th} \sim 60^{th}$	1	20.23	4.95	$25^{th} \sim 75^{th}$	1	19.78	4.15	5.27
20240221_F1	$25^{th} \sim 75^{th}$	1	16.63	3.47	$10^{th} \sim 90^{th}$	1	5.59	5.01	3.41
20240223_F1	$35^{th} \sim 65^{th}$	1	18.29	7.19	$25^{th} \sim 75^{th}$	1	7.95	6.13	1.1
20240223_F2	$40^{th} \sim 60^{th}$	1	11.53	2.73	$10^{th} \sim 90^{th}$	1	6.66	4.24	/
20240225	$30^{th} \sim 70^{th}$	1	29.92	2.29	$40^{th} \sim 60^{th}$	1	17.59	2.04	/
20240226_F2	$30^{th} \sim 70^{th}$	1	30.9	2.95	$30^{th} \sim 70^{th}$	1	8.81	4.4	3.12

Supplement 3 Sensitivity test of SSA end-member

Values of 0.90, 0.92, 0.95, 098, and 1 were selected to evaluate the sensitivity of mixing ratio model results. These values represent the variation between measurement and theoretical pure SSA_a. Flight 1 from March 23, 2024, was selected to evaluate the sensitivity of mixing ratio model results. On that day, 3 plume sampling periods were performed, and the SD method flagged 529 spikes. The proportion of spikes classified as containing more than 40%, 60%, and 80% SSA_a was recalculated for each threshold value. The results show that the fraction of spikes containing more than 40% SSA_a remained unchanged. Differences were observed for the highest SSA_a fraction (>80%), where lower threshold values resulted in a larger proportion of spikes being classified as highly SSA_a-dominated (10.7%).

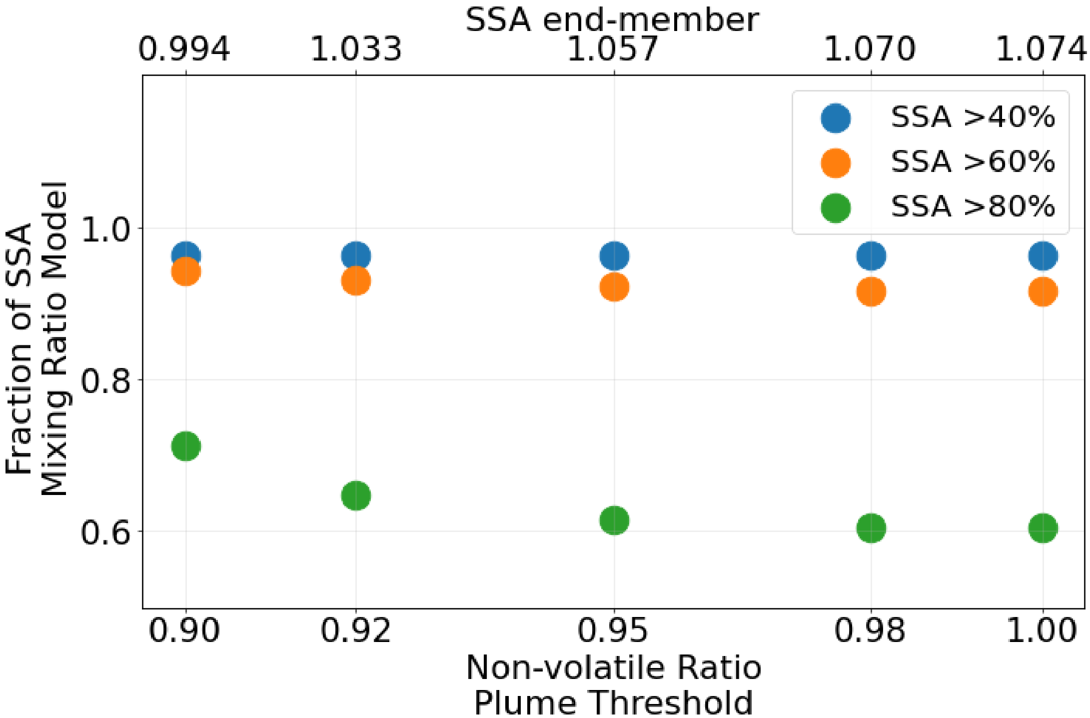

Figure S4 Sensitivity of sprayed SSA_a plume detection to mixing ratio model for flight1 on March 23rd, 2024. Plume fraction containing more than 40%, 60%, and 80% of sprayed SSA_a from the mixing ratio model was shown for different non-volatile ratio thresholds and SSA_a end-members (50th percentile).

Supplement 4 Uncertainty of mixing ratio model

The mixing ratio model was first evaluated by examining the separation between SSA_a and exhaust end-members under conservative uncertainty bounds, using ±20% reported by Matson et al. (2004). This difference is among different models of MCPCs, where in this study, we used the same MCPC model manufactured by Brechtel. The uncertainty is ±8% (Quinn et al., 2024). Applying a -20% to the lowest SSA_a non-volatile ratio (0.85) resulted in a value of 0.68, while applying a 20% to the highest exhaust non-volatile ratio (0.40) yielded a value of 0.48. The absence of overlap between these ranges demonstrates that the separation between SSA_a and exhaust remains robust even under conservative assumptions.

To investigate the uncertainty of the mixing ratio model, the propagation uncertainty in non-volatile aerosol ratio (±11.3%) was applied to a range of non-volatile aerosol ratios, as shown in Figure S5. The resulting uncertainty in SSA_a fraction from the mixing ratio model increased with increasing non-volatile aerosol ratio. The increased uncertainty should not affect the interpretation of mixing ratio model results, as the estimated SSA_a fraction remained sufficiently distinct to differentiate SSA_a-dominated from exhaust-dominated conditions.

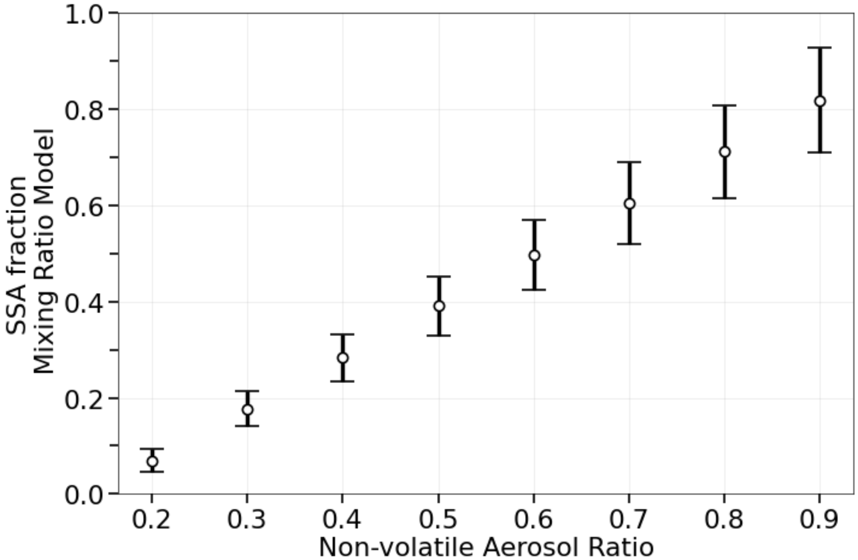

Figure S5 Uncertainty of SSA_a fraction from the mixing ratio model to non-volatile aerosol ratios. The circle represents the SSA_a fraction for each mixing ratio model input non-volatile aerosol ratio, and the error bar indicates the propagated uncertainty by applying the ±11.3% uncertainty to each non-volatile aerosol ratio.

References

El Yazidi, A., Ramonet, M., Ciais, P., Broquet, G., Pison, I., Abbaris, A., Brunner, D., Conil, S., Delmotte, M., Gheusi, F., Guerin, F., Hazan, L., Kachroudi, N., Kouvarakis, G., Mihalopoulos, N., Rivier, L., and Serça, D.: Identification of spikes associated with local sources in continuous time series of atmospheric CO, CO₂ and CH₄, Atmospheric Meas. Tech., 11, 1599–1614, https://doi.org/10.5194/amt-11-1599-2018, 2018.

Matson, U., Ekberg, L. E., and Afshari, A.: Measurement of Ultrafine Particles: A Comparison of Two Handheld Condensation Particle Counters, Aerosol Sci. Technol., 38, 487–495, https://doi.org/10.1080/02786820490462200, 2004.

Quinn, P. K., Bates, T. S., Coffman, D. J., Johnson, J. E., and Upchurch, L. M.: Use of an uncrewed aerial system to investigate aerosol direct and indirect radiative forcing effects in the marine atmosphere, Atmospheric Meas. Tech., 17, 3157–3170, https://doi.org/10.5194/amt-17-3157-2024, 2024.